Dalton Transactions

ROYAL SOCIETY OF CHEMISTRY

PAPER

View Article Online
View Journal

Cite this: DOI: 10.1039/d5dt02027a

Flux crystal growth of potassium lanthanide double vanadates with lanthanide-dependent coordination number variance

Hunter B. Tisdale [a,b] and Hans-Conrad zur Loye *[a,b]

Received 23rd August 2025,
Accepted 29th December 2025

DOI: 10.1039/d5dt02027a

rsc.li/dalton

A series of potassium rare earth double vanadates is presented. Single crystals of double vanadates with stoichiometry $K_3Ln(VO_4)_2$ (Ln = La, Pr, Nd, and Sm) and crystallizing in the glaserite structure type were synthesized *via* a molten alkali chloride/fluoride flux reaction. Different structures were observed depending on the constituent rare earth: $K_3La(VO_4)_2$ crystallizes in an as-of-yet unreported modification of the typical glaserite structure in the space group $P2_1/c$, likely due to its larger ionic size that results in an increase in the lanthanide coordination number (seven to eight). The Pr, Nd, and Sm compositions are isostructural with their phosphate analogues and crystallize in the space group $P2_1/m$. A discussion of the synthetic details, structure determination, structure descriptions, and coordination number variance is presented.

Introduction

Alkali rare earth double phosphates with stoichiometry $A_3Ln(PO_4)_2$ (A = Na, K, Rb, Cs) have demonstrated wide ranging properties and structural diversity that have made them attractive targets for ongoing research.[1–16] For example, both doped (dopants include Pr^{3+}, Gd^{3+}, Eu^{3+}, and Tb^{3+}) and undoped compositions have been synthesized and evaluated as potential photoluminescent materials.[2,4,17,18] Also, it has been shown that by varying the size of the constituent alkali and lanthanide elements, different structures may be obtained that vary in lanthanide content, coordination numbers, and symmetries.[5,10,16,18] Recently, the lanthanide double phosphates containing K^+ or Rb^+ have shown promise as potential nuclear waste forms for the sequestration of transuranic elements, such as americium,[10,19] as have other lanthanide phosphates, such as monazites.[20] Lanthanide phosphates, in general, (not just the double phosphates) have been of interest for their radiation tolerance, which make them ideal for nuclear waste forms requiring persistent materials.[10]

One of the most common structure types that the double phosphates crystallize in is the glaserite, $K_3Na(SO_4)_2$, structure.[12] The full lanthanide(III) series (excluding Pm) of $K_3Ln(PO_4)_2$ has been synthesized and published by Farmer *et al.*,[16] and we recently continued this work by synthesizing and publishing the full lanthanide(III) series (excluding Ce and Pm) of $Rb_3Ln(PO_4)_2$.[10] The majority of these phases crystallize in the monoclinic glaserite structure, however, for the smaller (heavier) lanthanides, a reduction in coordination number (seven to six coordination) for the constituent lanthanide with a change from to monoclinic to trigonal symmetry is observed. For the potassium analogues, this drop in coordination number occurs between Yb and Lu, while for the rubidium analogues, this change occurs between Tb and Dy. In addition, some double phosphates in the glaserite structure can by thermally induced to transition into this lower coordination number structure.[10,15] While this helps elucidate the influence of varying the alkali and lanthanide elements on the formation of specific structure types, significantly less work has been performed on varying the phosphate unit.

A structural unit with very similar chemistry to the phosphate, PO_4^{3-}, unit is the VO_4^{3-}, or vanadate, unit. Both the phosphorus and vanadium exist in their +5 oxidation state, have noble gas electron configurations, and form tetrahedral XO_4 units with 4 equal X–O bonds of order 1.25. This makes the vanadate unit an excellent candidate for substituting the phosphate unit in known compositions.[9,11,21–23] For example, the Kolis group has previously reported a series of potassium lanthanide double vanadates with the glaserite structure and stoichiometry $K_3Ln(VO_4)_2$.[22] They successfully synthesized the Sc, Y, and Dy–Lu analogues *via* both a supercritical hydrothermal and molten flux routes. However, the La–Tb analogues have yet to be reported in the literature. In this paper, we report the synthesis of the La, Pr, Nd, and Sm analogues of $K_3Ln(VO_4)_2$ *via* a molten flux route. The synthetic details, determination of their structures *via* single crystal X-ray diffraction, and structural details will be discussed.

[a]*Center for Hierarchical Waste form Materials, Columbia, South Carolina 29208, USA. E-mail: zurloye@mailbox.sc.edu*
[b]*Department of Chemistry and Biochemistry, University of South Carolina, Columbia, South Carolina 29208, USA*

Experimental

Reagents

La_2O_3 (Alfa Aesar, 99.9%), Nd_2O_3 (Acros Organics, 99.9%), Sm_2O_3 (Alfa Aesar, 99.99%), V_2O_5 (Alfa Aesar, 99.6%), KCl (Sigma Aldritch, 99.98%), and KF (Alfa Aesar, 99%) were used as received. Pr_6O_{11} (Alfa Aesar, 99.9%) was heated at 1000 °C for 12 h in an alumina crucible under H_2/N_2 gas flow to reduce it to the sesquioxide. The produced Pr_2O_3 was then used as is.

Synthesis

Single crystals of $K_3Ln(VO_4)_2$ were synthesized *via* a molten flux method. First, 1 mmol of Ln_2O_3, 2 mmol of V_2O_5, 11 mmol of KCl, and 9 mmol of KF were mixed thoroughly and added to a bowl-shaped platinum crucible. The crucible was then covered with a platinum lid and loaded into a programmable furnace. The furnace was then programmed to heat to 875 °C, dwell at 875 °C for 12 h, cool to 500 °C at 10 °C h^{-1} and finally shut off. The crucible was then allowed to cool to room temperature before removing it from the furnace. The crystals were extracted from the flux by sonicating the crucible in deionized water for 1 h and finally removing the dissolved flux *via* suction filtration.

Powder X-ray diffraction (PXRD)

A Bruker D2 Phaser equipped with a LYNXEYE XE-T silicon strip detector and a sealed-tube Cu K_α anode was used to collect PXRD data over a 2θ range of 5° to 65° on all products to determine phase identities and purities. The high energy resolution of the LYNXEYE XE-T detector allowed for energy cut-off of the K_β X-rays.

Single crystal X-ray diffraction (SXRD)

Single crystal X-ray diffraction data were collected on all $K_3Ln(VO_4)_2$ products at ambient temperature using a Bruker D8 QUEST diffractometer equipped with a microfocus IμS 3.0 sealed-tube X-ray source (Mo $K_{\alpha1}$, λ = 0.71073 Å) and a PHOTON II CPAD detector. Collected frames were integrated using SAINT+ and were corrected for absorption effects using SADABS in the Bruker APEX 3 software suite.[24] Initial structure models were obtained with SHELXT using intrinsic phasing[25] and refined with SHELXL using least-squares full-matrix methods[26] in OLEX2. Space groups were determined using a combination of XPREP systematic absences analysis[24] and ADDSYM (PLATON software suite) analysis.[27] Crystallographic information can be found in Table 1.

Results and discussion

Synthesis

A eutectic mixture of KCl and KF was utilized as a flux for the crystallization of $K_3Ln(VO_4)_2$. A ratio of 11 : 9 of KCl : KF corresponds to the approximate ratio at which their eutectic is at its minimum melting temperature: about 600 °C. By taking advantage of this lower melting point, the range of temperatures during which crystallization may occur is extended. Also, the use of an alkali halide flux provides both a source of K^+ for

Table 1 Crystallographic data for $K_3Ln(VO_4)_2$ (Ln = La, Pr, Nd, Sm)

Formula	$K_3La(VO_4)_2$	$K_3Pr(VO_4)_2$	$K_3Nd(VO_4)_2$	$K_3Sm(VO_4)_2$
System	Monoclinic	Monoclinic	Monoclinic	Monoclinic
Space group	$P2_1/c$	$P2_1/m$	$P2_1/m$	$P2_1/m$
a (Å)	7.6047(1)	7.5663(1)	7.5519(2)	7.5342(2)
b (Å)	5.9188(1)	5.9128(1)	5.9169(1)	5.9090(2)
c (Å)	20.0090(4)	9.9436(2)	9.9126(2)	9.8642(2)
β (°)	90.914(1)	90.895(1)	90.872(1)	90.809(1)
V (Å^3)	900.50(3)	444.80(1)	442.88(2)	439.11(2)
Z	4	2	2	2
Crystal size (mm^3)	0.1 × 0.1 × 0.05	0.08 × 0.08 × 0.04	0.38 × 0.35 × 0.15	0.1 × 0.1 × 0.1
Temperature (K)	297	299	301	299
D_x (g cm^{-3})	3.585	3.644	3.685	3.763
θ range (°)	2.9–36.3	2.7–36.3	2.7–36.3	3.4–36.3
Abs. coef. (mm^{-1})	8.09	8.86	9.26	10.12
Reflections collected	101 214	54 234	60 332	59 529
Independent reflections	4320	2316	2303	2260
R_{int}	0.026	0.035	0.043	0.028
h	$-12 \le h \le 12$	$-12 \le h \le 12$	$-12 \le h \le 12$	$-11 \le h \le 12$
k	$-9 \le k \le 9$	$-9 \le k \le 9$	$-9 \le k \le 9$	$-9 \le k \le 9$
l	$-33 \le l \le 33$	$-16 \le l \le 16$	$-16 \le l \le 16$	$-16 \le l \le 16$
$\Delta\rho_{max}$ (e$^-$ Å^{-3})	0.94	0.83	1.67	1.05
$\Delta\rho_{min}$ (e$^-$ Å^{-3})	−0.55	−0.66	−3.09	−1.13
Goodness-of-fit on F^2	1.31	1.16	1.42	1.41
$R_1(F)$ for $F_o^2 > 2\sigma(F_o^2)$	0.013	0.011	0.022	0.013
w$R_2(F_o^2)$	0.034	0.029	0.058	0.035
R_1(all)	0.014	0.012	0.022	0.013
wR_2(all)	0.035	0.029	0.058	0.035
F(000)	896	452	454	458
Extinction coefficient	0.00819(18)	0.0112(5)	0.300(6)	0.229(3)
Restraints/parameters	0/128	0/80	0/80	0/80

incorporation into products and a source of halides that may facilitate the solvation of the starting reagents. The Ln_2O_3 and V_2O_5 are unlikely to dissolve without the presence of such halides due to their high stabilities. Many fluxes, such as hydroxide salts, are prone to oxidizing constituents of the melt that have stable, lower oxidation states. In contrast, the alkali halide fluxes tend to be redox neutral which is necessary to maintain the correct oxidation states of the Ln(III) and V(V). As a result, high-quality, large, prismatic crystals were formed.[28]

Kolis *et al.* have previously reported difficulties in synthesizing the La through Tb analogues of $K_3Ln(VO_4)_2$ *via* molten flux and supercritical hydrothermal techniques.[22] However, they have reported using 1000 °C as their dwelling temperature for their flux reactions, while we have utilized a temperature of 875 °C to successfully synthesize the La through Sm analogues. Thus, there is likely a strong dependence of double vanadate crystallization on reaction temperature with a preference of lower temperatures for the lighter lanthanides. However, the Ce, Eu, Gd, and Tb analogues have not yet been successfully synthesized. For Ce, the reason is likely due to the instability of Ce^{3+} in open air at high temperatures. For Eu, Gd, and Tb, on the other hand, the reason for failure is less clear.

Unfortunately, all but the La reaction yielded impurities despite attempts at adjusting reaction parameters to select for $K_3Ln(VO_4)_2$ (Fig. 1 and 2). The amount of impurity formed increases across the series, suggesting that the smaller ionic size for later lanthanide ions leads to a mix of products. The impurity has been identified as a potassium lanthanide vanadate fluoride which will be discussed in a future publication.

Structure description

For Ln = Pr, Nd, and Sm, $K_3Ln(VO_4)_2$ crystallizes in the space group $P2_1/m$ and is isostructural with its phosphate analogues.[9] This structure is analogous to the glaserite structure and consists of $Ln(VO_4)_2$ 2D layers separated by K_3 layers in an ABAB... repeating sequence (Fig. 3). The $Ln(VO_4)_2$ layers consist of LnO_7 trigonal antiprisms and VO_4 tetrahedra. Each Ln(III) cation is bound to six VO_4 tetrahedra: five *via* corner sharing (monodentate) and one *via* edge sharing (bidentate). The Ln polyhedra do not share any anions with each other and

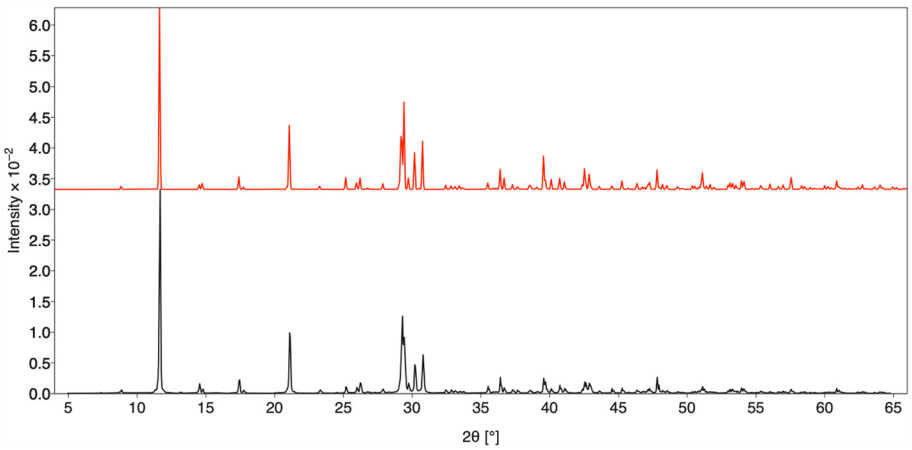

Fig. 1 PXRD of $K_3La(VO_4)_2$ (black) with simulated PXRD pattern calculated from SXRD model of $K_3La(VO_4)_2$ (red).

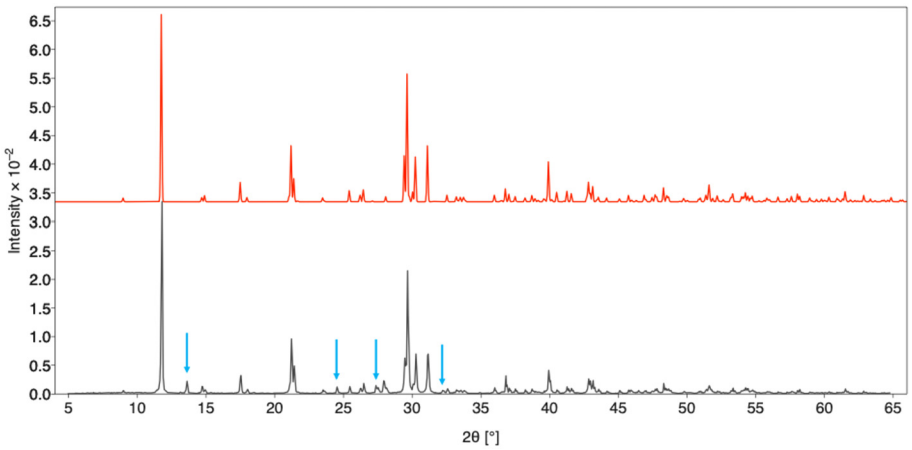

Fig. 2 PXRD of $K_3Sm(VO_4)_2$ (black) with simulated PXRD pattern calculated from SXRD model of $K_3Sm(VO_4)_2$ (red). Peak corresponding to impurities are indicated with blue arrows.

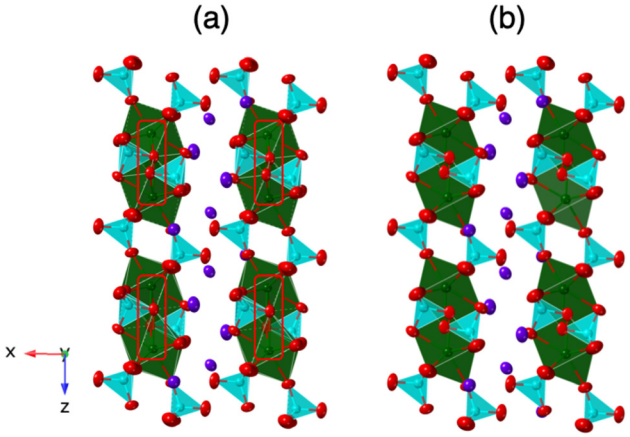

Fig. 3 View down the *b*-axis of $K_3Ln(VO_4)_2$ for (a) Ln = La and (b) Ln = Pr, Nd, and Sm. Ellipsoids are shown at 99% probabilities. The additional Ln–O bonds, relative to the 7-coordinate glaserite structure, are outlined in red.

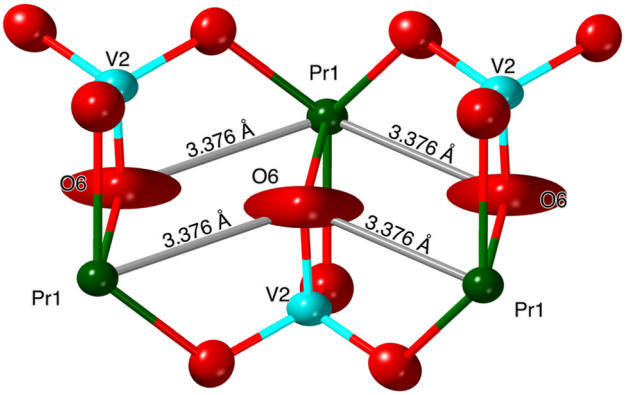

Fig. 5 Structure of typical monoclinic glaserite Ln–O6 chains showcasing the elongated O6 thermal ellipsoids and their distances to neighboring Ln atoms ($K_3Pr(VO_4)_2$ structure model shown).

the VO_4 tetrahedra do not interconnect. All O atoms are part of a VO_4 tetrahedron (Fig. 4). The K^+ layer, on the other hand, consists of three sublayers of K^+ atoms in a ccp arrangement. For Ln = La, however, $K_3Ln(VO_4)_2$ crystallizes in the space group $P2_1/c$ and is a modification of the typical glaserite structure (Fig. 3).

In the $K_3Ln(VO_4)_2$ models for Ln = Pr, Nd, and Sm, the thermal ellipsoid for O6 is elongated perpendicularly to the bond it creates with the Ln and extends towards two adjacent Ln atoms (Fig. 4 and 5). This phenomenon has been observed previously in the glaserite-type K^+ and Rb^+ alkali phosphates.[10,16]

In the $K_3La(VO_4)_2$ structure, this O atom (O8 in the La structure) no longer has an elongated ellipsoid but instead coordinates fully to one of the adjacent Ln atoms (Fig. 4). This changes the O atom from being bound to one V atom and one Ln atom to being bound to one V atom and two Ln atoms (Fig. 6 and 7). Consequently, the coordination number of La is eight instead of the typical seven in the glaserite structure. The elongated O ellipsoid in the $K_3Ln(VO_4)_2$ models for Ln = Pr, Nd, and Sm implies the possible presence of an attractive force between the adjacent Ln atoms and the elongated O that only becomes strong enough to lock into one position upon the incorporation of La. Due to the lanthanide contraction, shielding of 4f-electrons, and equivalent Ln charges (+3), this is likely to be a consequence of the larger size of La compared to Pr, Nd, and Sm. What is especially striking, however, is that O8 is shifted in a symmetrical fashion throughout the structure (Fig. 7). Looking down the *b* direction, the direction of the O8 shift from its standard glaserite position is constant for a single line of O8 atoms extending down the *b* direction. However, looking down the *c* direction, the O8 atoms alternate between shifting in the positive and negative *b* directions (Fig. 3). This symmetry doubles the unit cell size relative to the glaserite unit cell. Despite this doubling, no superstructure peaks at low 2θ are visible on the observed PXRD patterns.

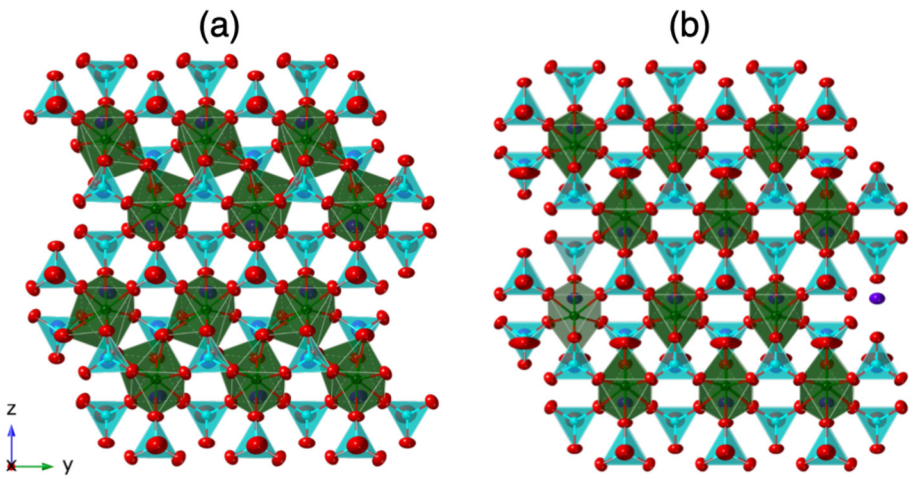

Fig. 4 View down the *a*-axis of $K_3Ln(VO_4)_2$ for (a) Ln = La and (b) Ln = Pr, Nd, and Sm. Ellipsoids are shown at 99% probabilities.

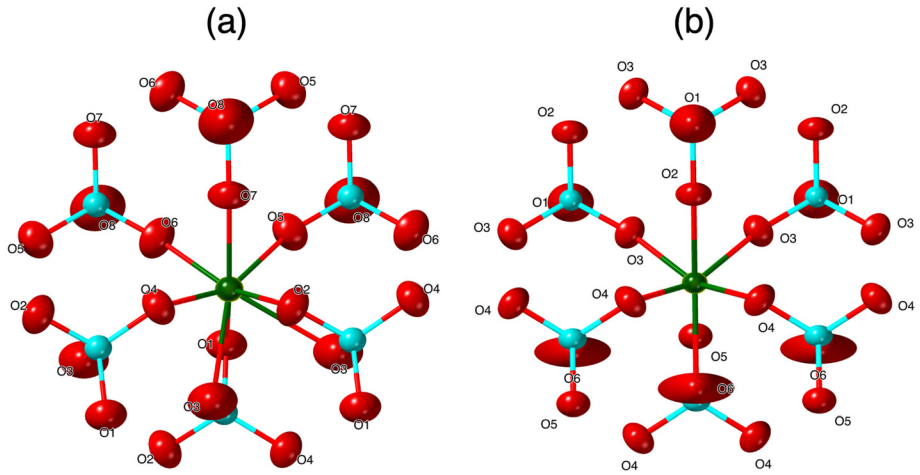

Fig. 6 Coordination environment of Ln in $K_3Ln(VO_4)_2$ looking down the *b*-axis for (a) Ln = La and (b) Ln = Pr, Nd, and Sm. Ellipsoids are shown at 99% probabilities.

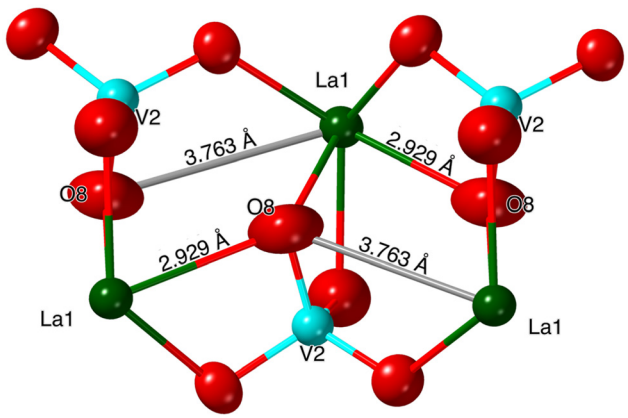

Fig. 7 Structure of $K_3La(VO_4)_2$ La–O8 chains showcasing the La–O8 distances.

Summary

Single crystals of $K_3Ln(VO_4)_2$ (Ln = La, Pr, Nd, and Sm) were synthesized *via* a molten KCl/KF eutectic flux. Challenges still exist in the synthesis of the full lanthanide(III) series with no successful attempts made at synthesizing high-quality single crystals of the Ce, Eu, Gd, and Tb analogues. The La analogue crystallizes in a novel modification of the glaserite structure with an increase in coordination number of the lanthanide from seven to eight. The Pr, Nd, and Sm products are all isostructural with their phosphate analogues. This change in coordination number is likely due to the significant difference in sizes of the lanthanides with La being the largest. Future work will focus on identifying new synthetic methods for targeting the Ce, Eu, Gd, and Tb analogues.

Conflicts of interest

There are no conflicts to declare.

Data availability

Raw data for other measurements are available upon request.

Supplementary information (SI) is available. See DOI: https://doi.org/10.1039/d5dt02027a.

CCDC 2480797–2480800 contain the supplementary crystallographic data for this paper.[29a–d]

Acknowledgements

Research was conducted by the Center for Hierarchical Waste Form Materials (CHWM), an Energy Frontier Research Center (EFRC). Research was supported by the U.S. Department of Energy, Office of Basic Energy Sciences, Division of Materials Sciences and Engineering under award DE-SC0016574.

References

1 A. J. Pelczarska and I. Szczygieł, Characteristics of hydrothermally obtained $Na_3RE(PO_4)_2$ phosphates, where RE = La, Ce, Nd, Gd or Er, *J. Therm. Anal. Calorim.*, 2022, **147**, 9913–9922.

2 R. Salmon, C. Parent, M. Vlasse and G. Le Flem, The crystal structure of a new high Nd concentration laser material: $Na_3Nd(PO_4)_2$, *Mater. Res. Bull.*, 1978, **13**, 439–444.

3 Q. Jing, M. Hu, M. Zhu, J. Wang, H. Duan and Z. Chen, Structure and optical properties of alkali rare-earth double phosphates of $M_3RE(PO_4)_2$ (M = K, Rb; RE = Y, La, and Lu), *Opt. Mater.*, 2024, **157**, 116278.

4 H. B. Tisdale, R. L. Conner, L. G. Jacobsohn and H.-C. zur Loye, Alkali rare earth double phosphates: Promising new high temperature scintillators, *Solid State Sci.*, 2024, **154**, 107612.

5 Y. Wang, Z. Lian, X. Su, Z. Yang, S. Pan, Q. Yan and F. Zhang, $Cs_6RE_2(PO_4)_4$(RE = Y and Gd): two new members

of the alkali rare-earth double phosphates, *New J. Chem.*, 2015, **39**, 4328–4333.
6 L. Schwarz, B. Finke, M. Kloss, A. Rohmann, U. Sasum and D. Haberland, Investigations on the electronic structure of double phosphates of the type $M_3RE(PO_4)_2$ (RE = rare earths, lanthanides), *J. Lumin.*, 1997, **72–74**, 257–259.
7 J. Legendziewicz, M. Guzik and J. Cybińska, VUV spectroscopy of double phosphates doped with rare earth ions, *Opt. Mater.*, 2009, **31**, 567–574.
8 S. H. Smith and B. M. Wanklyn, Flux growth of rare earth vanadates and phosphates, *J. Cryst. Growth*, 1974, **21**, 23–28.
9 M. Vlasse, C. Parent, R. Salmon and G. Le Flem, in *The Structures of $Na_3Ln(XO_4)_2$ Phases (Ln = Rare-Earth, X = P, V, As)*, Springer US, 1980, pp. 195–201.
10 H. B. Tisdale, M. S. Christian, G. Morrison, T. M. Besmann, K. Sun, G. S. Was and H.-C. zur Loye, Investigation of Rare Earth-Containing Double Phosphates of the Type $A_3Ln(PO_4)_2$ (Ln = Y, La, Pr, Nd, and Sm–Lu) as Potential Nuclear Waste Forms, *Chem. Mater.*, 2022, **34**, 3819–3830.
11 P. P. Mel'nikov and L. H. Komissarova, Double phosphates, arsenates, and vanadates of rare earth elements, scandium, and yttrium with alkali metals, *Dokl. Akad. Nauk SSSR*, 1981, **256**, 878–881.
12 V. A. Eframov, P. P. Mel'nikov and L. N. Komissarova, New compounds of the glaserite type, *Rev. Chim. Miner.*, 1985, **22**, 666–675.
13 P. P. Mel'nikov, V. B. Kalinin, V. A. Efremov and L. N. Komissarova, Double orthophosphates of rare earths (Gd-Lu), yttrium and scandium with rubidium, *Izv. Akad. Nauk SSSR, Neorg. Mater.*, 1981, **17**, 1452–1455.
14 J. M. Farmer, L. A. Boatner, B. C. Chakoumakos, C. J. Rawn, D. Mandrus, R. Jin and J. C. Bryan, Polymorphism, phase transitions, and thermal expansion of $K_3Lu(PO_4)_2$, *J. Alloys Compd.*, 2014, **588**, 182–189.
15 S. V. Ushakov, A. Navrotsky, J. M. Farmer and L. A. Boatner, Thermochemistry of the alkali rare-earth double phosphates, $A_3RE(PO_4)_2$, *J. Mater. Res.*, 2004, **19**, 2165–2175.
16 J. M. Farmer, L. A. Boatner, B. C. Chakoumakos, C. J. Rawn and J. Richardson, Structural and crystal chemical properties of alkali rare-earth double phosphates, *J. Alloys Compd.*, 2016, **655**, 253–265.
17 M. Trevisani, K. V. Ivanovskikh, F. Piccinelli and M. Bettinelli, Fast 5d-4f luminescence in Pr^{3+}-doped $K_3Lu(PO_4)_2$, *J. Lumin.*, 2014, **152**, 2–6.
18 D. Zhao, F.-X. Ma, P.-G. Duan, C.-K. Nie, J.-F. Guo and R.-J. Zhang, Commensurately modulated structure and luminescent properties of $Na_3Pr(PO_4)_2$, *J. Lumin.*, 2017, **192**, 129–135.
19 T. K. Deason, H. B. Tisdale, A. T. Hines, G. Morrison, Y. Zhoujin, M. D. Smith, T. M. Besmann, A. M. Mofrad, S. L. Estes, J. W. Amoroso, D. P. DiPrete and H.-C. zur Loye, Investigation of Americium-Containing Phosphates, Silicates, Borates, Molybdates, and Fluorides Synthesized via High-Temperature Flux Crystal Growth, *J. Am. Chem. Soc.*, 2025, **147**, 21659–21671.
20 Y. Zhoujin, H. B. Tisdale, N. Keerthisinghe, G. Morrison, M. D. Smith, J. Hadermann, T. M. Besmann, J. Amoroso and H.-C. Z. Loye, A low-temperature, one-step synthesis for monazite can transform monazite into a readily usable advanced nuclear waste form, *Sci. Adv.*, 2025, **11**, eadt3518.
21 K. Byrappa, C. K. Chandrashekar, B. Basavalingu, K. M. LokanathaRai, S. Ananda and M. Yoshimura, Growth, morphology and mechanism of rare earth vanadate crystals under mild hydrothermal conditions, *J. Cryst. Growth*, 2007, **306**, 94–101.
22 M. M. Kimani, L. Thompson, W. Snider, C. D. McMillen and J. W. Kolis, Hydrothermal synthesis and spectroscopic properties of a new glaserite material, $K_3RE(VO_4)_2$ (RE = Sc, Y, Dy, Ho, Er, Yb, Lu, or Tm) with potential lasing and optical properties, *Inorg. Chem.*, 2012, **51**, 13271–13280.
23 M. M. Kimani, C. D. McMillen and J. W. Kolis, Synthetic and spectroscopic studies of vanadate glaserites II: Photoluminescence studies of $Ln:K_3Y(VO_4)_2$ (Ln=Eu, Er, Sm, Ho, or Tm), *J. Solid State Chem.*, 2015, **226**, 320–325.
24 *APEXIII Version 2016.5–0, SAINT Version 8.37A, SADABS Version 2016/2*, 2016.
25 G. M. Sheldrick, SHELXT - Integrated space-group and crystal-structure determination, *Acta Crystallogr., Sect. A: Found. Adv.*, 2015, **71**, 3–8.
26 G. M. Sheldrick, Crystal structure refinement with SHELXL, *Acta Crystallogr., Sect. C: Struct. Chem.*, 2015, **71**, 3–8.
27 A. L. Spek, Single-crystal structure validation with the program PLATON, *J. Appl. Crystallogr.*, 2003, **36**, 7–13.
28 D. E. Bugaris and H.-C. zur Loye, Materials Discovery by Flux Crystal Growth: Quaternary and Higher Oxides, *Angew. Chem., Int. Ed.*, 2012, **51**, 3780–3811, DOI: 10.1002/anie.201102676.
29 (*a*) CCDC 2480797: Experimental Crystal Structure Determination, 2026, DOI: 10.25505/fiz.icsd.cc2p8gq5; (*b*) CCDC 2480798: Experimental Crystal Structure Determination, 2026, DOI: 10.25505/fiz.icsd.cc2p8gr6; (*c*) CCDC 2480799: Experimental Crystal Structure Determination, 2026, DOI: 10.25505/fiz.icsd.cc2p8gs7; (*d*) CCDC 2480800: Experimental Crystal Structure Determination, 2026, DOI: 10.25505/fiz.icsd.cc2p8gt8.